Measuring asymmetry with AFNI

Daniel R. Glen[1], Kadharbatcha Saleem[2], Richard C. Reynolds[1], Paul A. Taylor[1]

[1]Scientific and Statistical Computing Core (NIMH, NIH, USA), [2]Section on Quantitative Imaging and Tissue Sciences (NICHD,NiH, USA)

Contact: glend @ mail.nih.gov Web: https://afni.nimh.nih.gov/pub/dist/doc/htmldoc/

NIH National Institutes of Health NIH National Institute of Mental Health

OHBM 2026 BORDEAUX JUNE 14–18 FRANCE

OHBM-2026
Poster #2456
Wednesday, June 17 | 13:45-14:45
Thursday, June 18 | 14:45-15:45

Introduction: Asymmetry

Investigations of symmetry and asymmetry are commonly performed in structural and functional MRI to help identify the differences between right and left-brain properties. These may be useful to help characterize disease, development and evolution. Here, we describe a new program in AFNI [Cox 1996] to quickly compute a number of useful quantities that include morphological differences in volume, surface area of regions and the surface area of the regions projected onto a common surface (e.g., cortex).

Methods: Looking for asymmetry in volumes and surface areas

The new program, asymm_report.csh, computes the various shape-related quantities and outputs a clear report with the columns of values. To run the analysis, the user provides the program with lists of both right and left-side region indices, along with a volumetric dataset containing the regions. Optionally, surfaces can be provided for left-right queries, such as those generated with FreeSurfer [Fischl 2012] and SUMA [Saad 2012]. Alternatively, the surfaces can be automatically generated from the volumetric data as isosurfaces via the IsoSurface program in AFNI.

Figure 1 shows visualizations of the three types of asymmetries that are computed for a pair of regions, using the AFNI and SUMA GUIs. The purely volumetric differences are the most straightforward to evaluate, counting voxels for each of the left regions and the right regions with multiplication by the voxel size for the volume using 3dBrickStat. The ratio of right to left volumes are included in the output by default with options for laterality index (left-right)/(left+right). The surfaces of each region can be generated using an isosurface rendering of the labeled volume, and the surface areas are estimated from these for each region using SUMA's SurfaceMetrics; the ratios between right and left areas are then computed and output analogously to the volumetric measures. A typical way to compute surface area is to project volumetric parcellations onto a common surface like the cortex surface from FreeSurfer; the surface area is then computed as the area of the patch of surface the labelled parcellation covers with SUMA's SurfMeasures.

We present an example here to evaluate the asymmetries of the cerebellar structures across three species - marmoset (MBMv3.0) [Liu, 2018], macaque (NMTv2.1) [Jung 2021] and human (MNI_2009c_asymmetric) [Fonov 2011] using the atlases we have recently developed for the cerebellum [Saleem 2021].

Results: Asymmetry of cerebellums across primate species

Asymmetry was measured for the cerebellum across recently introduced atlases for different species with reports shown for each. An example report is shown in Fig. 1 for the macaque cerebellum in the NMT 2.1 template space, and the Sim_p (Posterior part of the simple lobule) region is highlighted. Here we can see the regions are nearly symmetric in terms of volumetric and region isosurface areas (i.e., the R/L ratios are near 1), but they have much less symmetric patch surface areas, with a R/L ratio of 0.58.

In Figure 2, the comparison of the volumetric asymmetry ratio shows the marmoset and macaque with relatively symmetric cerebellums compared with the human MNI template. Each of these were parcellated with our recently introduced atlases for each of the species. Extending the analysis over an available group of 134 subjects from 6 different sites, scanners and age ranges shows similar asymmetries in select regions (Figure 3).

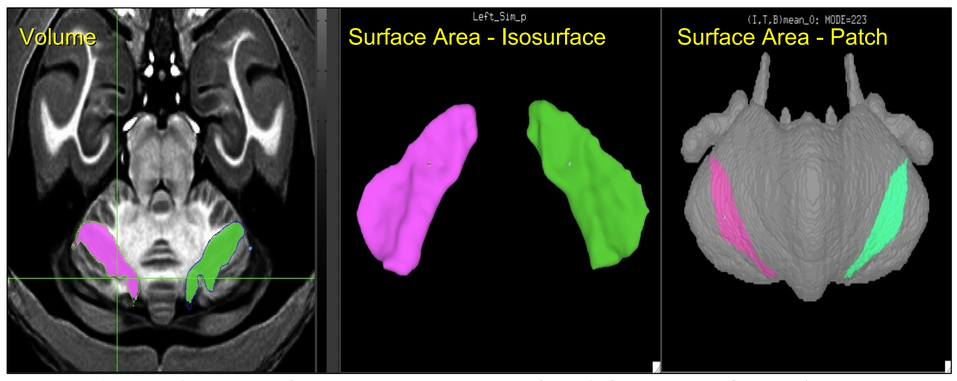


Figure 1. Visualizations of Asymmetry. Regions of the left and right Sim_p (posterior part of the simple lobule) are shown as three types of regional representations for visualization and quantification. Panel A shows a volume with a slicewise view in AFNI, where volumetric measures are made in mm^3. Panels B and C each show mesh-based renderings using SUMA, where surface measures are made in mm^2. Panel B shows the regional isosurface renderings, and Panel C shows regions projected onto a common surface.

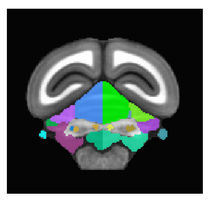
Simple Syntax :

```
asymm_report.csh -input $sub                              \
   -right_range 1 21 -left_range 31 51                    \
   -reportfile  ${asymm_dir}/${subname}_asymm.txt
```

For the two kinds of surface asymmetries, these options could be added to compute isosurfaces and measures of asymmetry:

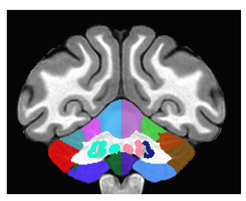
```
   -isosurf_dir $isosurf_dir/${subname}                   \
   -isosurf_base $subname                                 \
   -surf_patch -make_patch_surface
```

Marmoset
MCA atlas
MBM v3 template



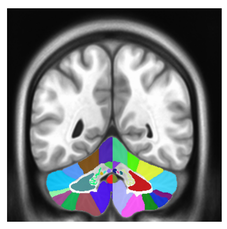
#index	label	right_vol	left_vol	r/l_asymm
61	DN	1.2	1.2	1.021
62	AIN	0.8	0.9	0.863
63	PIN	0.8	0.8	1
64	FN	1.3	1.2	1.101
108	I	1	1	0.976
109	II	8.1	9.5	0.852
110	III	15.4	15.8	0.978
111	IV	18.2	17.4	1.046
112	V	40.6	39.3	1.035
113	VI	26.8	24.7	1.086
114	VII	22.2	20.4	1.089
115	VIII	13.9	12.5	1.116
116	IX	15.9	15.2	1.047
117	X	8.1	8.5	0.96
118	Par_p	22.5	19.7	1.142
119	Par_a	27.5	29	0.945
120	Cr_II	22.5	18.6	1.211
121	Cr_I	4.9	3.9	1.263
125	FI	21.6	21	1.028
217	MCP	9.5	8.7	1.1
222	Sim_a	8.3	9.7	0.858
223	Sim_p	14	15.4	0.914
233	PFI	12	11	1.086

Macaque
D99 atlas
NMT template



#index	label	right_vol	left_vol	r/l_asymm
61	DN	44.5	45.4	0.979
62	AIN	17	18.4	0.922
63	PIN	14.9	16.1	0.925
64	FN	19.2	20.8	0.922
108	I	16.8	16.1	1.046
109	II	65.4	69.7	0.937
110	III	187.4	202.8	0.924
111	IV	211	205.1	1.029
112	V	439.5	408.2	1.076
113	VI	150.5	134.8	1.116
114	VII	109.7	105	1.044
115	VIII	93.5	86.6	1.079
116	IX	115.4	104.5	1.105
117	X	39.7	36.8	1.079
118	Par_p	206.5	229.9	0.898
119	Par_a	186	192.4	0.967
120	Cr_II	255.8	230.6	1.109
121	Cr_I	300.8	315.3	0.954
123	PFI	243.5	235.3	1.035
124	Cop	372.7	362.5	1.028
125	FI	37.3	39.7	0.94
153	scp	7.9	6	1.317
217	mcp	102.7	103.8	0.989
222	Sim_a	135.5	147.4	0.919
223	Sim_p	208.9	187	1.117

Human
HCA Atlas
MNI 2009b template



#index	label	right_vol	left_vol	r/l_asymm
1	I/II	60.6	100.1	0.605
2	III	915	988.6	0.926
3	IV	4098.4	3693.2	1.11
4	V	3753.5	6044.4	0.621
5	VI	11850.1	10475	1.131
6	VIIA-f/t	194.4	371.6	0.523
7	VIIB	7365.8	7315.9	1.007
8	VIIIA	6653.6	7174	0.927
9	VIIIB	5427.4	5975.6	0.908
10	IX	4331	4968.5	0.872
11	X	596.2	713.4	0.836
12	Cr_I	19665.8	18644.6	1.055
13	Cr_II	11263.4	11516.9	0.978
14	DN	616.4	568.6	1.084
15	EN	45.6	40	1.141
16	GN	8.8	8.6	1.014
17	FN	44	52.1	0.844
18	SCP	366.9	361.6	1.015
19	MCP	2672.1	2432.6	1.098
20	ICP	135.9	135.8	1.001
21	CWM	3801.2	3269.4	1.163

Figure 2. Asymmetry of the cerebellum across three primate species - marmoset, macaque and human



Asymmetry of cerebellum across human population of 134 subjects

#Idx	ROI	right	left	total	r/l_asymm			ra/la_asymm			rpa/lpa_asymm		
#	label	vol	vol	vol	min	max	mean	min	max	mean	min	max	mean
1	I/II	42.49	68.36	110.85	0.39	0.87	0.63	0.07	0.75	0.39	0.00	100.00	7.81
2	III	668.59	714.63	1383.23	0.68	1.24	0.95	0.87	1.16	1.02	0.28	4.94	1.28
3	IV	3113.95	2793.49	5907.44	0.87	1.39	1.12	0.94	1.17	1.06	0.36	3.75	1.08
4	V	2676.21	4425.09	7101.30	0.43	0.79	0.61	0.66	0.88	0.77	0.20	1.90	0.52
5	VI	8756.92	7831.44	16588.36	0.85	1.39	1.12	0.94	1.18	1.06	0.25	2.34	1.08
6	VIIA-f/t	160.30	308.90	469.20	0.38	0.65	0.52	0.51	0.80	0.67	0.00	100.00	10.36
7	VIIB	6160.48	6037.32	12197.80	0.75	1.38	1.02	0.85	1.09	0.98	0.14	2.54	0.82
8	VIIIA	5369.54	5878.55	11248.09	0.70	1.23	0.92	0.80	1.04	0.92	0.31	2.26	0.98
9	VIIIB	4486.22	5004.08	9490.30	0.60	1.33	0.90	0.76	1.14	0.90	0.22	4.88	0.99
10	IX	3336.70	3909.50	7246.20	0.57	1.22	0.86	0.79	1.10	0.94	0.28	3.20	1.09
11	X	558.12	633.77	1191.89	0.64	1.18	0.88	0.77	1.07	0.91	0.35	3.59	1.17
12	Cr_I	15549.50	15095.50	30645.00	0.87	1.18	1.03	0.93	1.13	1.01	0.17	7.11	0.99
13	Cr_II	8871.50	9071.29	17942.79	0.70	1.23	0.98	0.86	1.08	0.99	0.28	3.21	1.17
14	DN	427.47	388.38	815.85	0.76	1.57	1.11	0.73	1.48	1.10	0.38	4.22	1.37
15	EN	29.09	26.52	55.61	0.64	2.83	1.14	0.11	34.00	1.60	0.07	100.00	4.04
16	GN	5.59	5.86	11.45	0.20	4.00	1.07	0.00	100.00	6.97	0.00	100.00	14.86
17	FN	28.72	34.36	63.08	0.36	1.53	0.86	0.06	3.84	0.77	0.09	21.99	1.51
18	SCP	264.25	271.81	536.06	0.78	1.26	0.98	0.83	1.17	0.97	0.28	3.82	1.48
19	MCP	2017.32	1843.51	3860.83	0.87	1.31	1.10	0.91	1.18	1.03	0.30	2.70	1.11
20	ICP	107.60	101.87	209.47	0.51	1.82	1.08	0.69	1.51	1.04	0.22	3.85	1.42
21	CWM	3008.67	2519.60	5528.27	1.01	1.42	1.20	0.99	1.27	1.13	0.20	2.75	1.20

Figure 3. Asymmetry of cerebellum regions across human population, 134 subjects, 6 sites, various age ranges and scanner types. HCA atlas applied to individual subject brains. Volume, surface area, surface patch area asymmetry ratios are shown. Notably larger asymmetries highlighted in red.

Conclusions

Quantifying anatomical asymmetry is fundamental to studies of brain organization, development, evolution, and disease, yet few tools provide a straightforward framework for comprehensive asymmetry analysis. The new AFNI program, asymm_report.csh, addresses this need by offering an automated and flexible approach for measuring volumetric, isosurface, and surface-projected asymmetries from labeled neuroanatomical regions.

By integrating automatic surface generation with multiple asymmetry metrics, the program enables rapid and reproducible characterization of left-right differences across species and populations. While surface-based measures can provide complementary information, their interpretation depends on regional geometry, proximity to the reference surface, and the accuracy of surface generation and label projection. Consequently, volumetric and surface-derived metrics should be considered together to obtain a more complete picture of anatomical asymmetry.

Our cross-species analyses demonstrate that marmoset and macaque cerebellums are relatively symmetric, whereas the human cerebellum exhibits pronounced asymmetries in several regions. Similar patterns were observed across a diverse cohort of 134 human subjects, highlighting the robustness of these findings.

By providing a simple, scalable, and comprehensive framework for asymmetry assessment, asymm_report.csh has the potential to facilitate large-scale studies of normative brain organization and to identify structural phenotypes associated with neurological and neurodevelopmental disorders.

Acknowledgments and References

This work utilized the computational resources of the NIH HPC Biowulf cluster (http://hpc.nih.gov).

1. Taylor PA, Glen DR, Reynolds RC, Basavaraj A, Moraczewski D, Etzel JA (2023). Front. Neurosci. 17:1205928.
2. Cox RW (1996). Comput Biomed Res 29:162-173.
3. Fischl B. FreeSurfer. Neuroimage. 2012;62(2):774-781.
4. Jung B, Taylor PA, Seidlitz J, et al. A comprehensive macaque fMRI pipeline and hierarchical atlas. Neuroimage. 2021;235:117997.
5. Kerestes R, Han S, Balachander S, et al. A Standardized Pipeline for Examining Human Cerebellar Grey Matter Morphometry using Structural Magnetic Resonance Imaging. J Vis Exp. 2022;(180):10.3791/63340. Published 2022 Feb 4.
6. Liu C, Ye FQ, Yen CC, et al. A digital 3D atlas of the marmoset brain based on multi-modal MRI. Neuroimage. 2018;169:106-116.
7. Nettekoven, C., & Diedrichsen, J. (2025). Cerebellar asymmetries. Handbook of Clinical Neurology, 208, 369-378.
8. Saad ZS, Reynolds RC. SUMA. Neuroimage. 2012;62(2):768-773.
9. Saleem KS, Avram AV, Glen D, et al. High-resolution mapping and digital atlas of subcortical regions in the macaque monkey based on matched MAP-MRI and histology. Neuroimage. 2021;245:118759.

RR, DG, and PT were supported by the NIMH Intramural Research Program (ZICMH002888) of the NIH/HHS, USA. KS was supported by the NICHD Intramural Research Program (IRP) and the NIH BRAIN Initiative 1U01EB026996-01.The contributions of the NIH authors were made as part of their official duties as NIH federal employees, are in compliance with agency policy requirements, and are considered Works of the United States Government; however, the findings and conclusions presented in this paper are those of the authors and do not necessarily reflect the views of the NIH or the U.S. Department of Health and Human Services.